Classification of an Exposed Mixed-Sediment Tidal Flat Using Synthetic Aperture Radar

Julie Paprocki[1#], *Nina* Stark[2], *Fred* Falcone[3], and *Hans C.* Graber[4]

[1]*University of New Hampshire Department of Civil and Environmental Engineering, 33 Academic Way, Kingsbury Hall W139, Durham, NH 03824, USA*
[2]*University of Florida, Engineering School for Sustainable Infrastructure and Environment, 265H Weil Hall, Gainesville, FL 32611, USA*
[3]*Virginia Tech, Department of Civil and Environmental Engineering, 200 Patton Hall, 750 Drillfield Drive, Blacksburg, VA 24061, USA*
[4]*Center for Southeastern Tropical Advanced Remote Sensing, Rosenstiel School of Marine, Atmospheric, and Earth Science, University of Miami, 11811 SW 168th St, Miami, FL, 33177, USA*
[#]*Corresponding author: julie.paprocki@unh.edu*

ABSTRACT

Estuarine tidal flats represent a critical environment for maintaining healthy ecosystems. The geotechnical characterization of such environments is often challenging due to their soft nature and remote locations. Thus, the goal of this study is to explore the use of remotely sensed, high resolution (pixel resolution of ~0.5 m) synthetic aperture radar (SAR) data for characterizing these sediments. Towards this goal, the variability of sediment properties (median gain size, moisture content, fines content, and classification following the Unified Soil Classification System (USCS) were documented for a mixed tidal flat located on the Great Bay Esturay in New Hampshire, USA. A sediment classification scheme based on SAR, originally proposed by Gade et al. (2008), which utilizes the correlation length to characterize sediments based on the percentage of particles <0.063 mm, was tested using a high-resolution X-band SAR image (pixels of ~0.5 m) collected simultaneously to in situ measurements and a medium-resolution C-band image (pixels of ~10 m) collected 3 days later. The results of this study demonstrate that the framework proposed by Gade et al. (2008) was generally able to predict the correct soil classification for coarser sediments but failed to predict the correct soil classification for finer sediments when applying the original image resolutions. When the X-band image was downsampled to match the C-band image resolution, the framework was still unable to predict the expected soil classification. This suggests that, in order to utilize high-resolution X-band data to predict soil type, alternative sediment type classification schemes are required.

Keywords: remote sensing; mixed sediments; synthetic aperture radar

1. Introduction

Tidal flats are critical coastal environments that support healthy ecosystems and protect coastal communities from erosion. Management strategies of tidal flats and estuarine environments require a detailed understanding of tidal flat sediments, including the geotechnical characteristics and the spatial sediment classification. However, due to their soft nature and location, tidal flats can be challenging to access and traditional testing may be difficult to perform. New advances in remotely sensed satellite data may be able to provide information regarding the geotechnical characterization of tidal flats on large spatial extents.

Previously, it has been demonstrated that synthetic aperture radar (SAR), an active remote sensing technique, can be used to characterize the soil composition of tidal flats using images with pixel sizes >10 m (Choe and Kim 2011; Deroin 2012; Gade et al. 2008; Lee et al. 2012; van der Wal et al. 2005). However, modern advances have resulted in SAR images with sub-meter pixel resolutions that have not been tested for such applications. SAR, an active remote sensing technique, is

able to image through clouds and storm events. Unlike passive remote sensing techniques like optical systems, they transmit their own energy source through a series of pulses. After hitting the ground, some of this energy is returned to the satellite and is referred to as backscatter. For bare soils, the backscatter is related to the radar properties (wavelengths, incidence angle, and polarization, which refers to the plane in which the transmitted and received signals are polarized) and terrain properties (dielectric properties of the soil-air-water mixture, surface roughness, orientation of the features imaged). The surface roughness, in turn, is characterized by three parameters: the standard deviation of the height (or RMS height), correlation length, and correlation function (Davidson et al. 2000; Ulaby et al. 1986). Of most importance are the rms height, which describes the random variation of the surface with respect to some mean surface, and the correlation length, which describes the horizontal distance over which the roughness profile is autocorrelated with some value larger than 0.368 (or $1/e$) (Ulaby et al. 1986).

For exposed intertidal flats, it has been demonstrated that, since they are often saturated, information regarding the soil texture can be derived from C-band SAR images

Figure 1. (a) Overview of the Great Bay Estuary, showing the location of Mast Cove; (b) overview of Mast Cove site, denoting the location of the coarser (lighter markers) and finer (darker markers) zones.

(van der Wal et al. 2005). Other studies have employed the use of decision trees for X-band data (Lee et al. 2012) or by inverting SAR models (Choe and Kim 2011; Deroin 2012; Gade et al. 2008) to classify the sediment type. The method proposed by Gade et al. (2008) to characterize soil type of mixed tidal flats from SAR suggested to invert the Integral Equation Model (IEM) (Fung et al. 1992) in conjunction with multi-frequency data to estimate the correlation length. This method makes two major assumptions: first that the backscatter response is primarily controlled by the profile of sand ripples and secondly that the rms height and correlation length can be used as proxies for the sediment type. This technique, along with others, were developed and tested on low to medium resolution data (pixel sizes on the order of tens of meters) and for only a single polarization. Furthermore, the technique of Gade et al. (2008) was tested for a site where sand was dominated by ripples and was not tested for when the site is composed of predominantly muddy sediments. Finally, such techniques have not been tested for high-resolution data. Thus, the goal of this study is to test the applicability of the sediment scheme proposed by Gade et al. (2008) on an exposed tidal flat not dominated by ripples on the Great Bay Estuary in southeastern New Hampshire, USA using high-resolution X-band SAR data.

2. Methods

2.1. Regional Context

The Great Bay Estuary (Fig. 1a), located within the Gulf of Maine, is a drowned river valley located in New Hampshire in the northeastern United States. At the mouth of the estuary, the tidal range is 2.5 m and decreases in the bay to 1.8 m (Bilgili et al. 2003), with the water volume changing by approximately 40% during low tide (Ertürk et al. 2002). As a result, approximately 50% of the fringing tidal flats are exposed at low tide (Bilgili et al. 2005; Cook et al. 2019). The Lower Piscataqua River region of the Great Bay, where Mast Cove is located (Fig. 1b), stretches from New Castle Island, NH on the Gulf of Maine, to Dover Point, NH. This portion of the estuary is a highly dissipative region that behaves like a partially progressive wave and has

strong maximum tidal currents of up to 2 m/s (Cook, Lippmann, and Irish 2019; Swift and Brown 1983). The strong tidal currents prevent most fine sediments from being deposited, resulting in a high percentage of coarse (>0.075 mm grain size) sediments in Mast Cove.

2.2. Sediment Sampling

In total, 22 sediment samples were collected at low tide using 10 cm tall by 6.67 cm diameter transparent tubes (Fig. 2) at eleven stations. Two samples were collected at each station. The samples were processed for water contents, grain sizes following ASTM 6913 (ASTM 2017b), and were classified following the Unified Soil Classification System (USCS). Due to the percentage of fines found at Mast Cove, samples were also processed via wet sieving following ASTM 1140 (ASTM 2017a). Dry sieving was performed using the No. 4 (4.75 mm), 10 (2.00 mm), 20 (0.85 mm), 40 (0.425 mm), 100 (0.150 mm), and 200 (0.075 mm) sieves following wet sieving. Atterberg limits were performed on the fines content from Mast Cove to measure the liquid and plastic limits following ASTM 2487 (ASTM 2005). Water contents were measured by drying ~100 g of soil for 24 hours at 100°C in an oven and weighing the samples before and after drying. Water contents were not corrected for organic matter or salt content.

Figure 2. Example of a sediment sample collected at Mast Cove

2.3. Satellite Image Processing

Concurrent to sampling, a horizontally co-polarized X-band SAR image from the Cosmo-SkyMED-4 (CSK4; see Table 1 for details) satellite was collected during low tide when the sediments were exposed to air (Fig. 3). The

image was collected at an incidence angle of 38.1°. Images were first corrected to the backscatter coefficient, σ^o, from the digital number, DN, using the open-source Sentinel-1 toolbox for the Sentinel Application Platform (SNAP) (Veci 2019).
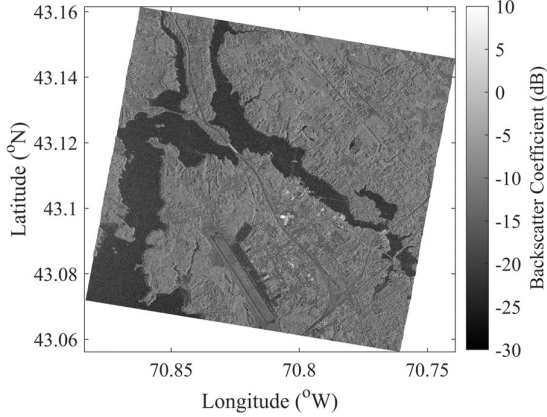

Figure 3. Cosmo-SkyMED-4 image of the Great Bay Estuary on 06 August 2021 at 22:36 UTC. COSMO-SkyMed Product - ©ASI - Agenzia Spaziale Italiana - 2021. All Rights Reserved.

Since backscatter can span multiple orders of magnitude, it is typically expressed logarithmically:

$$\sigma^o_{dB} = 10 \cdot \log_{10}(\sigma^o) \qquad (1)$$

where σ^o_{dB} is the backscatter in units of dB. Images were then geometrically corrected using the STRM 1 sec HGT DEM (Veci 2019).

After calibration, the soil type of the tidal flat was determined on a per-pixel basis using the approach of Gade et al. (2008). In this technique, the integral equation model (IEM) (Fung et al. 1992) was used in conjunction with multi-frequency SAR data (i.e. data collected over different wavelength) to classify soils following the scheme proposed by Pröber (1981). This scheme groups sediments based on the percentage of microparticles (grain size <0.063 mm) as sand (microparticles <10%), mixed (microparticles 10%-25%) and mixed/muddy (microparticles >25%). The correlation length is estimated using look up tables (LUTs) generated for the backscatter over different SAR frequencies and finding their intersection. Then, this estimated correlation length is used to classify sediments using 3.7 cm as the boundary between mixed and sandy soils and 4.2 cm to distinguish between mixed and mixed/muddy soils.

The physical IEM model (Fung et al. 1992) calculates the backscatter of a bare soil as a function of the dielectric constant (ϵ), RMS height in cm (s), the correlation function (ρ), correlation length in cm (L), polarization (VV, VH, or HH), radar wavenumber (k), and incidence angle in radians (θ), with the general form expressed as (Fung and Chen 2004):

$$\sigma^o_{pp} = \frac{k^2}{4\pi}\exp\left(-2k^2s^2\cos^2\theta\right)$$
$$* \sum_{n=1}^{+\infty} |I^n_{pp}|^2 \frac{W^{(n)}(2k\sin\theta, 0)}{n!} \qquad (2)$$

where $p = $ v or h, $W^{(n)}$ is the is the Fourier transform of the nth power of the surface correlation function ρ, and

$$I^n_{pp} = (2ks*\cos\theta)^n f_{pp}\exp(-k^2s^2\cos^2\theta)$$
$$+ (ks*\cos\theta)^n F_{pp} \qquad (3)$$

For horizontally co-polarized backscatter, f_{pp} and F_{pp} are calculated using Eqns 4 and 5:

$$f_{pp} = f_{hh} = -\frac{2R_h}{\cos\theta} \qquad (4)$$

$$F_{pp} = F_{hh} = 2\frac{\sin^2\theta}{\cos\theta}\left[4R_h \right.$$
$$\left. - \left(1 - \frac{1}{\epsilon}\right)(1 + R_h)^2\right] \qquad (5)$$

where ϵ is the complex dielectric constant and R_h is the horizontally polarized Fresnel reflection coefficient:

$$R_h = \frac{\cos(\theta) - \sqrt{\epsilon - \sin^2\theta}}{\cos(\theta) + \sqrt{\epsilon - \sin^2\theta}} \qquad (6)$$

The Fourier transform of the nth power of the surface correlation function is defined as:

$$W^{(n)}(a, b) = 2\pi \iint \rho^n(x, y)e^{-i(ax+by)}dxdy \qquad (7)$$

For this study, the correlation function was assumed to be Gaussian. Using this approach, multiple pairs of RMS height and correlation length can result in the same value of backscatter for a given moisture content.

Table 1. Summary of satellite characteristics

Sensor	Pixel Size	Frequency (band)	Polarization
Cosmo-SkyMED-4	0.5 m	9.6 GHz (X)	HH
Sentinel-1A	10 m	5.405 GHz (C)	VV

To apply the IEM model, the real (ϵ') and imaginary (ϵ'') parts of the complex dielectric constant ($\epsilon = \epsilon' - j\epsilon''$) were calculated for the measured moisture content using the Hallikainen et al. (1985) model:

$$\epsilon = a_0 + a_1 S + a_2 C + (b_0 + b_1 S + b_2 C)m_v$$
$$+ (c_0 + c_1 S + c_2)m_v \qquad (8)$$

where S and C are the percentage of sand and clay (by weight) of the soil, m_v is the volumetric moisture content, and a_i, b_i, and c_i are coefficients that are a function of the frequency from Hallikainen et al. (1985); the coefficients developed for 10 GHz were used.

To provide a crude estimate of the soil type, Gade et al. (2008) found that the correlation length could be estimated by inverting the IEM model (Fung et al. 1992) over multiple frequencies and using the same image resolution. They used images from the L- (frequencies of 1-2 GHz), C-, (frequencies of 4-8 GHz), and X-band data at HH-polarization to distinguish between soil types. Thus, at least one additional image is required to predict the soil type. For Mast Cove, an image was collected on 09 August 2021 at 22:35 UTC (three days after measurements) from the C-Band (frequency of 5.405 GHz) Sentinel-1A (S1A) satellite at an incidence angle of 34.9°; this image is shown in Fig. 4 with sensor details provided in Table 1. Both images were collected at similar tidal states, with the CSK4 image collected

approximately one hour following low tide and the S1A image collected approximately one hour preceding low tide (WillyWeather 2023). To calculate the dielectric constant, the coefficients for 6 GHz from Hallikainen et al. (1985) were used in Eqn. 8. For this study, no images at a third frequency were available for the site at the time of measurements.
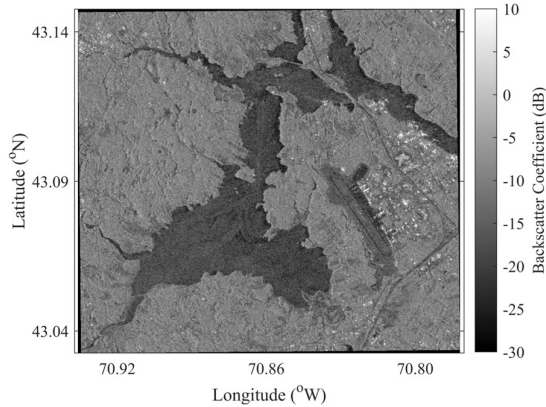

Figure 4. Sentinel-1A image of the Great Bay Estuary on 09 August 2021 at 22:35 UTC. Sentinel-1A product – © Copernicus Sentinel data – 2021.

To test if a difference in resolution impacts the predicted soil type, the X-band SAR image was downsampled to a pixel resolution of 10 m using the weighted average warping technique in QGIS (GDAL/OGR contributors 2024). The resulting soil classifications were then derived for two cases: (1) the backscatter from the images at their original resolutions and (2) using backscatter from the original resolution for the C-band image but the backscatter from the downsampled X-band image.

3. Results and Discussion

3.1. Sediment Samples

From classification testing, the fines at Mast Cove classify as non-plastic silt. The cross-flat trends in moisture content, percent fines (percentage by weight with a grain size <0.075 mm), and the median grain size d_{50} are shown in Fig. 5c-e, respectively, with the USCS classification for all samples shown in Table 2. The triangles represent the measurement obtained from the first sample while the circle represents the second sample collected at each station. The first set of points at 0 m refers to MC1 while the final set of points at 110.5 m represents MC11. All sediment samples classified as sandy following the USCS classification scheme. However, Mast Cove has two distinct sediment regions: one composed on a higher percentage of fines and moisture content (stations MC7 through MC11, referred to as the finer region) and one with generally lower fines percentages and moisture contents (stations MC1 through MC6, referred to as the coarser region).

All samples from the stations within the finer region of Mast Cove (stations MC7-MC11; Fig. 1b) classified as silty sands (SM), with fines content ranging from 14.1-33.2% (average of 26.0%). The water contents at these stations ranged from 26.5-38.3%, with an average of

34.2%. In general, the two samples at each station from this region exhibited similar values of d_{50}, with some variability in the moisture content and fines content.

Table 2. USCS classification for all samples collected at Mast Cove on 06 August 2023.

Station Name	Sample 1	Sample 2
MC1	SM	SP-SM
MC2	SP-SM	SM
MC3	SM	SM
MC4	SM	SM
MC5	SM	SM
MC6	SP-SM	SP
MC7	SM	SM
MC8	SM	SM
MC9	SM	SM
MC10	SM	SM
MC11	SM	SM

The stations in the coarser region of Mast Cove (stations MC1 through MC6) exhibited a wider range of characteristics and classifications than the finer region of Mast Cove. These samples had fines contents ranging from 4.1-39.6%, with an average of 17.1% and moisture contents ranging from 20.4-41.2%, with an average of 27.5%. For these samples, there was some variability in d_{50}, particularly near MC1 and MC2. Sample 1 from MC2 and sample 2 from MC1 and MC2 had gravel contents >15%, and thus carry "with gravel" in their full classification. Both samples generally resulted in similar values for the fines content, with some variability in the water content observed, again for samples from MC1 and MC2. A peak in moisture content and fines content as well as a decrease in d_{50} is observed at MC4 (distance of 35.7 m); this corresponds to crossing the draining channel seen in Fig. 1b. Stations MC3 and MC5 were also located near the drainage channels, which resulted in slightly higher values of moisture content and percentage of fines. Previous studies with samples collected near Mast Cove also suggest diverse classifications, with samples collected slightly offshore of the site having 91.5% sands and 8.5% silts/clays (particles <0.063 mm) (Mattera et al. 2022) and a sample collected over the flat as having 42.9% sands and 57.1% silts/clays (Poppe, 2003). Other samples from the site exhibit similar trends (Paprocki et al. 2024)

3.2. Satellite Image Processing

Fig. 5a presents the cross-flat trends in backscatter for the *HH*-polarized X-band image collected 06 August 2021 following the profile shown in Fig. 1b. The stars represent the measurement locations. From Fig. 5a, it is apparent that there are distinct trends in backscatter for the different regions of Mast Cove. For the coarser region (0-81 m), backscatter ranged from -29.0 dB to -2.1 dB, with an average of -14.1 dB. Lower backscatter coefficients were observed in the first 30.2 m with minimums in the range of -20 dB, which may be a result of ponded water in pillow-hollows observed during measurements. Local minima (-29.0 dB and -25.1 dB) were observed at distances of 31.3 m and 51.3 m, respectively. These locations likely correspond to crossing the drainage channels observed at the site (see
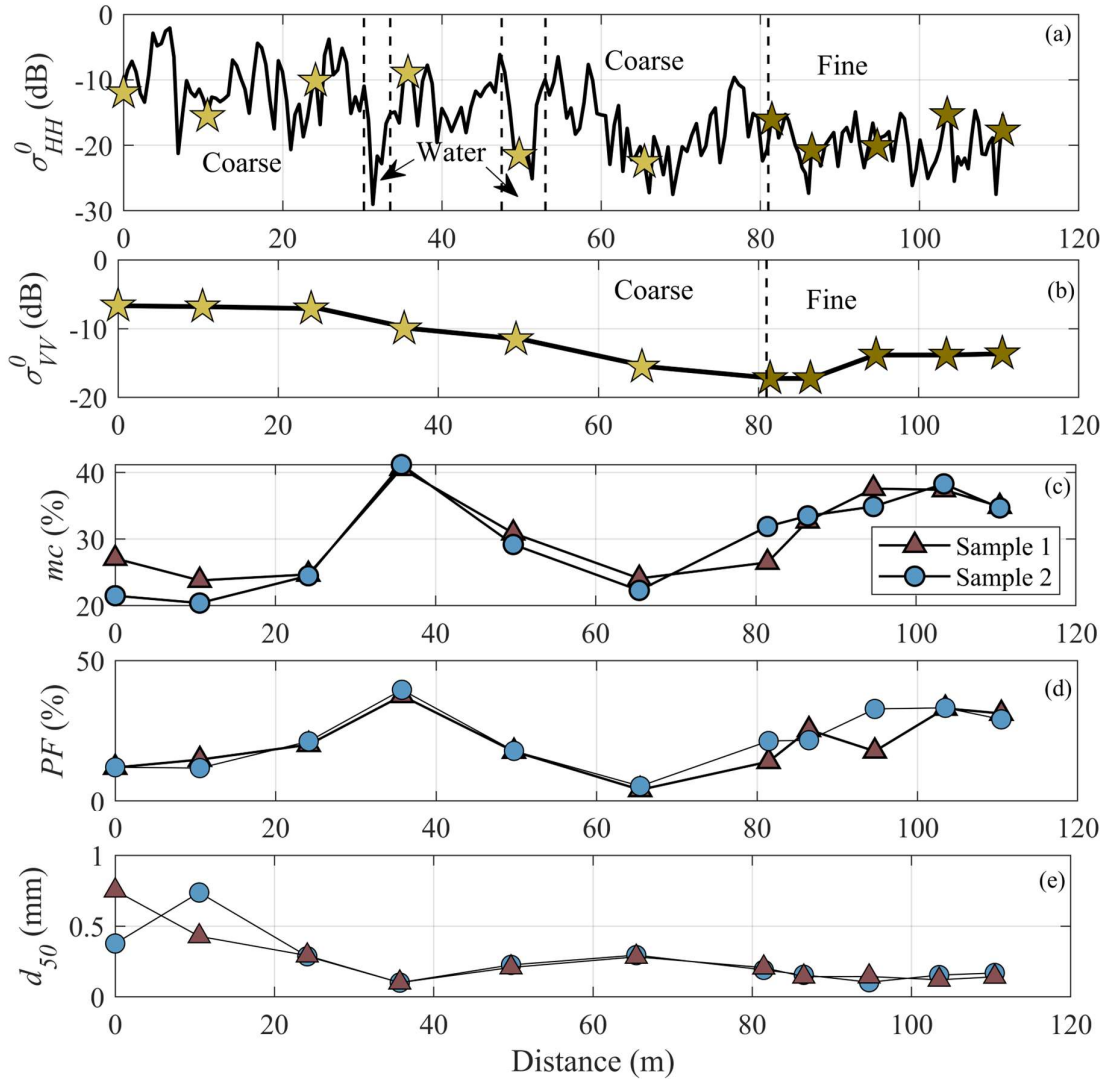
4

Figure 5. Trends in (a) horizontally co-polarized backscatter coefficient from the CSK4 image collected on 06 August 2021 at 22:36 UTC and an incidence angle of 38.1°, (b) vertically co-polarized backscatter coefficient from the Sentinel-1A image collected on 09 August 2021 at 22:35 UTC and an incidence angle of 34.9°, (c) measured moisture content, (d) percentage of fines (particles <0.075 mm), and (e) median grain size d_{50} in mm.

Fig. 1b). Backscatter values lower than the average were observed from 59.5 m to 81 m. Although this section of the profile is part of the coarser region, it was near the water line, which may have impacted the recorded backscatter. The backscatter for the finer region (81 m to 110.5 m) ranged from -27.5 dB to -13.8 dB, with an average of -19.8 dB.

Fig. 5b presents the cross-flat trends in vertically co-polarized backscatter for the C-band image collected 09 August 2021 following the profile shown in Fig. 1b. The highest values of backscatter were observed in the sandy region (average of -9.62 dB), with the highest values observed at MC1-MC3 (average of -6.86 dB). Slightly lower values were observed at MC4-MC6 (average of -12.38 dB); these stations were in the vicinity of the drainage channel (MC4 and MC5) and near the water line (MC6). The finer region of Mast Cove (stations MC7-MC12) exhibited lower average values of backscatter (average of -15.15 dB), with lower values observed at stations MC7 and MC8 than MC9-MC12.

Gade et al. (2008) found that, when soils were asaturated, the backscatter depended primarily on the surface roughness conditions, with lesser influence from the moisture and soil composition. Thus, a single LUT can be developed for tidal flats for a given frequency and incidence angle. For exposed sites, Gade et al. (2008) suggested to use pure sand and a volumetric moisture content of 43%. The LUT for X-band and an incidence angle of 38.1° is shown in Fig. 6 and the LUT for C-band and an incidence angle of 34.9° is shown in Fig. 7 using the suggested sand content and moisture content. The calculated isolines for each station based on the LUT shown in Fig. 6 for the X-band were compared to those derived for each station based on the in situ measurements of moisture content and fines content, with minimal differences found. The greatest differences were observed for the sandy sites, with less differences observed for the finer sites.

For each station, the correlation lengths were found by inverting the IEM model (Fung et al. 1992) using the

LUTs shown in Fig. 6 and Fig. 7. The isolines for each station were calculated using the average backscatter of a 3 pixel by three pixel block for the CSK4 image at its original resolution and the pixel value where the station was located for the S1A image and the CSK4 iamge when it was downsampled to a 10 m pixel resoltuion. These isolines were then plotted simultaneously, with examples shown in Fig. 8, with the intersection between the two isolines selected as the correlation length. When using the CSK4 image at its original resolition, four stations (MC1-MC4), which correspond to the coarser region of Mast Cove, had no intersection between the two isolines; an example of this for MC1 is shown in Fig. 8a. When using the downsampled CSK4 image, three stations (MC1-MC3) had no intersection. This may be a result of the factors such as the percentage of gravel materials or variations in mineralogy may have impacted the recorded backscatter. Gravel samples are able to more freely drain than sands or fines and such, may not be fully saturated during imaging and thus, this approach may not be applicable for these soils.
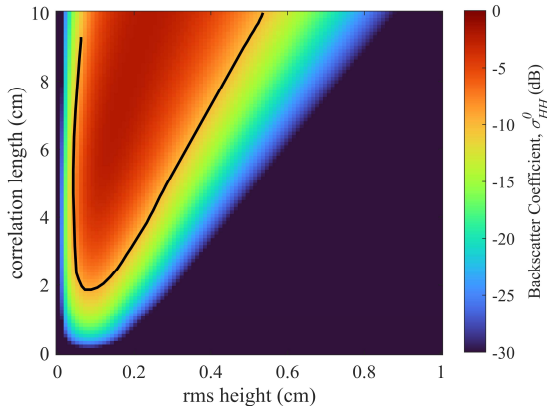

Figure 6. Visual representation of a LUT for *HH*-polarization, an incidence angle of 38.1°, sand content of 100%, and a moisture content of 43%. The solid black line represents the isoline for -10 dB.
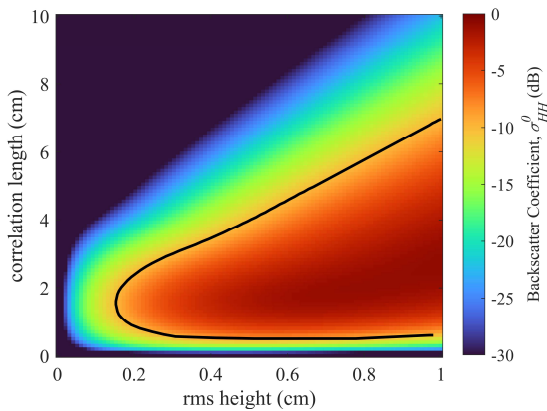

Figure 7. Visual representation of a LUT for *VV*-polarization, an incidence angle of 34.9°, sand content of 100%, and a moisture content of 43%. The solid black line represents the isoline for -10 dB.

The remaining eight stations when using the original CSK4 image resolution and nine stations when using the downsampled CSK4 image resulted in two intersections between the isolines (Fig. 8b). The higher value was selected as the correlation length, as shown by the arrow

in Fig. 8b. The resulting correlation lengths for these stations are presented in Fig. 9, with the circles representing the correlation length when using the backscatter from the original resolution of the CSK4 image while the squares represent the correlation length estimated using the backscatter from the downsampled CSK4 image. The dashed horizontal lines in Fig. 9 represent the boundaries defined by Pröber (1981) to discriminate between sands, mixed, and mixed/muddy sediments. Using these limits, two stations classify as mixed/muddy seediments sediments (MC6 and MC8) when using both the backscatter from the original CSK4 image resolution and the backscatter from the downsampled image. Two stations classified as mixed (MC7 and MC9) when using the backscatter from the original image resolution while four stations (MC5, MC9-MC11) classified as mixed when using the downsampled image backscatter. The remaining three classified as sands (MC5, MC10, and MC11) when using the original image resolution wile the remaining two (MC4 and MC5) classified as sands when using the downsampled resolution. When using the backscatter from the original CSK4 image, two stations classified as the expected soil type (MC5, MC8) while three stations (MC6, MC10, and MC11) did not classify as the expected soil type. Two stations, MC7 and MC9, classified as mixed while mixed/muddy sediments were expected. When using the backscatter from the downsampled CSK4 image, four stations (MC4-MC5, MC7-MC8) classified following the expected trends while the remaining four stations (MC6, MC9-MC11) did not classify according to the expected trends, with all stations classifying as mixed.
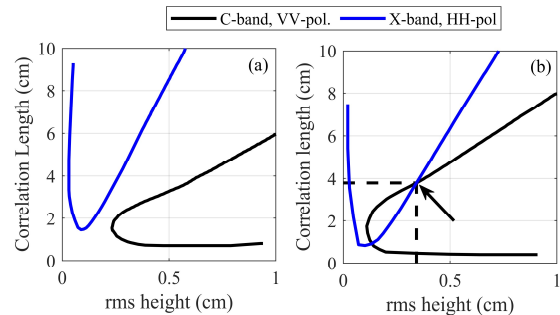

Figure 8. Examples of the inversion process used following Gade et al. (2008), with the X-band *HH*-polarized isoline shown in blue and the C-band *VV*-polarized isoline shown in black. (a) Station MC1 where there was no intersection point between the two isolines and (b) Station MC 9 where there were two intersection points between the two isolines.

Although different discrimiators were used to determine the fines content between Pröber (1981) and the present study, there are several discrepanies between the predicted and anticipated soil classifications. For example, station MC6 classifies as mixed mixed/muddy using the the backscatter from the downsampled and original CSK4 images, respectively, when using the scheme of Pröber (1981), which would suggest that the percentage of material <0.063 mm would be >25%. However, from wet sieving, the percenage of material <0.075 mm was measured to be 5.4% and 4.1% from the two samples (Fig. 5d), indicating a misclassification of the sediment. This misclassification may be a result of
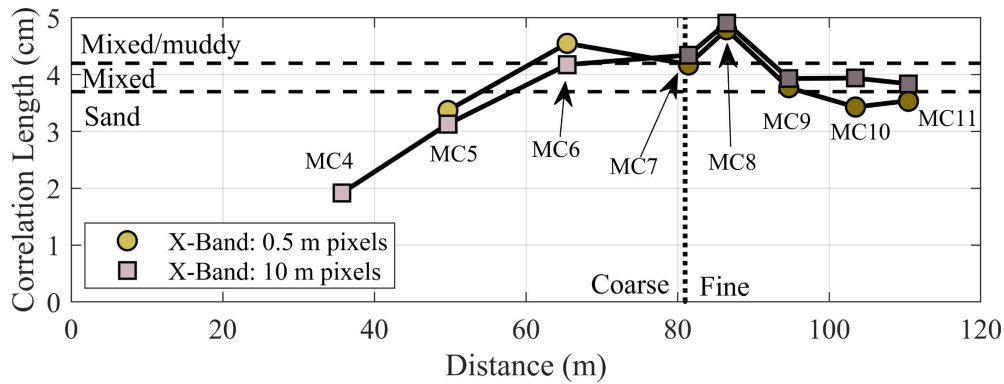
Figure 9. Estimated correlation lengths for Mast Cove. The dashed horizontal lines indicate the classification scheme defined by Pröber (1981) while the dotted vertical line represents the separation between the coarser (darker symbols) and finer (lighter symbols) regions of Mast Cove.

the proximity of the station to the water line, where water would influence the backscatter return. This would be especially true for the C-band image and the downsampled X-band iamge, where the backscatter response of this pixel represents the average conditions on the ground. For this station, water could have been included in that pixel, impacting the results.

Furthermore, station MC7 exhibited similar physical characteristics to MC8 in terms of moisture content, grain sizes, and fines content but exhibited different classifications and minor differences in the backscatter response when comparing the results obtained using the backscatter from the original CSK4 image. Similarly, stations MC9-MC11 exhibited similar moisture contents to MC8, but slightly higher fines contents, but were classified as different sediment classes using the limits of Pröber (1981). This suggests that other factors may be influencing the SAR backscatter beyond the soil classification, such as biological activity and mineralogy. However, this theory is under investigation, and will be the focus of future work.

A potential source of error in this study is the image resolution used in comparison to the fine-scale changes in sediment characteristics. The area studied by Gade et al. (2008) was significantly larger than the area studied here. For their study, Gade et al. (2008) using images with pixel resolutions of 12.5 m and demonstrated trends in backscatter for a profile length of ~2,000 m cross-shore. At Mast Cove the profile was only ~65.5 m cross-shore (Fig. 5; stations MC1-MC6). The backscatter recorded within a single pixel represents the average conditions over that pixel (Lillesand et al. 2015). Thus, due to the wide variability of ground conditions (Table 2, Fig. 5c-e), this average backscatter over this 100 m^2 pixel from the C-band is likely unable to allow for the small-scale changes observed at the site be to be observed and higher resolution images are required. As an alternative technique for characterizing sites, it may be possible to use the statistical trends in backscatter for the entire region to characterize the broad soil type. These relationships are currently under investigation, with a primary emphasis on the relationship between mean backscatter and uniformity (a measure of how uniform the backscatter values are) and entropy (a measure at how random the backscatter values are) (Paprocki 2024).

In the next phase of this work, measurements of the ground roughness characteristics, in conjunction with the grain size characteristics, will be conducted. This will allow for the development and calibration of a new classification scheme using the correlation length that accounts for the geotechnical classification and characterization of the sediments using high-resolution X-band SAR.

4. Conclusions

This study presents the distribution of sediment characteristics as well as trends in backscatter coefficients from both X-band and C-band SAR images for a mixed sediment tidal flat on the Great Bay Estuary in New Hampshire, USA towards the goal of classifying the exposed sediment using remote sensing. The site was composed of two distinct regions: a coarser region with a low percentage of fines and lower moisture contents, and a finer region with a higher fines contents and moisture contents. Similarly, the remotely sensed SAR data exhibited distinct trends for the two regions, with both the X-band and C-band SAR exhibiting higher backscatter values for the coarser region and lower values for the finer region.

Due to the trends in backscatter, it was tested if the framework proposed by Gade et al. (2008) could be used to classify the sediments. In this method, the correlation length is estimated using the Integral Equation Model (IEM) by Fung et al. (1992) and data from different sensors to classify the soil as sandy (microparticles <10%), mixed (microparticles between 10-25%), or mixed/muddy (microparticles > 25%). The backscatter response for each station was extracted, and isolines of those backscatters were developed for each satellite frequency, pure sands, and a moisture content of 43% (Figs. 6 and 7). This framework was tested for two cases: first, using the original resolution of both images and second, using a downsampled X-band image to match the resolution of the C-band image.

For both cases. the correlation length was unable to be estimated for four and three stations, respectively, which is likely due to the high percentage of gravels found at these stations. Of the remaining stations, four and three stations for the downsampled versus original backscatter classified according to the anticipated trends

while all remaining stations did not. For both cases original and downsampled backscatter, the classification at three stations (MC6, MC10, and MC11) conflicted with those determined from in situ measurements. Mismatches in the sediment classification may be a result of biological activity influencing the SAR backscatter, issues associated with the image resolution, and the soil mineralogy. In the future, in situ measurements of the roughness characteristics will be conducted in conjunction with sediment characterization and image collection to test if the framework proposed by Gade et al. (2008) can be adapted for the joint use of high-resolution X-band and medium-resolution C-band SAR of different resolutions for characterizing soil type of exposed intertidal flats.

Acknowledgements

References

ASTM. 2005. "Standard test methods for liquid limit, plastic limit, and plasticity index of soils." West Conshohocken, PA: ASTM. https://doi.org/10.1520/D4318-17E01.

ASTM. 2017a. "Standard test methods for amount of material in soils finer than the No . 200 (75-mm)." West Conshohocken, PA: ASTM. https://doi.org/10.1520/D1140-17.

ASTM. 2017b. "Standard test methods for particle-size distribution (gradation) of soils using sieve analysis." West Conshohocken, PA: ASTM. https://doi.org/10.1520/D6913-04R09.2.

Bilgili, A., M. R. Swift, D. R. Lynch, and J.T.C. Ip. 2003. "Modeling Bed-Load Transport of Coarse Sediments in the Great Bay Estuary, New Hampshire." Estuar. Coast. Shelf Sci., 58 (4): 937–50. https://doi.org/10.1016/j.ecss.2003.07.007.

Bilgili, A., J. A. Proehl, D. R. Lynch, K. W. Smith, and M. R. Swift. 2005. "Estuary/Ocean Exchange and Tidal Mixing in a Gulf of Maine Estuary: A Lagrangian Modeling Study." Estuar. Coast. Shelf Sci., 65 (4): 607–24. https://doi.org/10.1016/j.ecss.2005.06.027.

Choe, B.-H., and D. Kim. 2011. "Retrieval of Surface Parameters in Tidal Flats Using Radar Backscattering Model and Multi-Frequency SAR Data." Korean J. of Remote Sens., 27 (June). https://doi.org/10.7780/kjrs.2011.27.3.225.

Cook, S. E., T. C. Lippmann, and J. D. Irish. 2019. "Modeling Nonlinear Tidal Evolution in an Energetic Estuary." Ocean Model., 136 (April): 13–27. https://doi.org/10.1016/j.ocemod.2019.02.009.

Davidson, M. W. J., T. L. Toan, F. Mattia, G. Satalino, T. Manninen, and M. Borgeaud. 2000. "On the Characterization of Agricultural Soil Roughness for Radar Remote Sensing Studies." IEEE Trans. Geosci. Remote Sen., 38 (2): 630–40. https://doi.org/10.1109/36.841993.

Deroin, J.-P. 2012. "Combining ALOS and ERS-2 SAR Data for the Characterization of Tidal Flats. Case Study from the Baie Des Veys, Normandy, France." Int. J. of Appl. Earth Obs. Geoinf., 18 (August): 183–94. https://doi.org/10.1016/j.jag.2012.01.019.

Ertürk, Ş. N., A. Bilgili, M. R. Swift, W. S. Brown, B. Çelikkol, J. T. C. Ip, and D. R. Lynch. 2002. "Simulation of the Great Bay Estuarine System: Tides with Tidal Flats Wetting and Drying." J. Geophys. Res., 107 (C5): 3038. https://doi.org/10.1029/2001JC000883.

Fung, A. K., and K. S. Chen. 2004. "An Update on the IEM Surface Backscattering Model." IEEE Geosci. Remote Sens. Lett., 1(2): 75–77. https://doi.org/10.1109/LGRS.2004.826564.

Fung, A.K., Z. Li, and K.S. Chen. 1992. "Backscattering from a Randomly Rough Dielectric Surface." IEEE Trans. Geosci. Remote Sen., 30(2): 356–69. hppts://doi.org/10.1109/36.134085

Gade, M., W. Alpers, C. Melsheimer, and G. Tanck. 2008. "Classification of Sediments on Exposed Tidal Flats in the German Bight Using Multi-Frequency Radar Data." Remote Sens. of Environ., 112 (4): 1603–13. https://doi.org/10.1016/j.rse.2007.08.015.

GDAL/OGR contributors. 2024. GDAL/OGR Geospatial Data Abstraction Software Library. Open Source Geospatial Foundation. https://doi.org/10.5281/zenodo.5884351.

Hallikainen, M. T., F. T. Ulabz, M. C. Dobson, M. A. El-Rayes, and L. K. Wu. 1985. "Microwave Dielectric Behavior of Wet Soil-Part I: Empirical Models and Experimental Observations." IEEE Trans. Geosci. Remote Sen., GE-23 (1): 25–34. https://doi.org/10.1109/TGRS.1985.289497.

Lee, Y.-K., J.-W. Park, J.-K. Choi, Y. Oh, and J.-S. Won. 2012. "Potential Uses of TerraSAR-X for Mapping Herbaceous Halophytes over Salt Marsh and Tidal Flats." Estuar. Coast. Shelf Sci., 115 (December): 366–76. https://doi.org/10.1016/j.ecss.2012.10.003.

Lillesand, J., R. W. Kiefer, and J. Chipman. 2015. Remote Sensing and Image Interpretation. Hoboken, N.J.: John Wiley and Sons.

Mattera, T., D. M Burdick, L. Martin, A. Giacchetti, S. Kehoe, K. Matso, T. Gregory, and C. Hays. 2022. "Tier 2 Monitoring in the Great Bay Estuary, NH/ME Field Season 2021." 460. PREP Reports & Publications. https://scholars.unh.edu/prep/460.

Paprocki, J., N. Stark, T. Lippman, and H. C. Graber. 2024. "Geotechnical Investigation of Exposed Intertidal Flats at the Great Bay Estuary Using Sediment Sampling and Satellite-Based Synthetic Aperture Radar." J. Waterw. Port Coast. Ocean Eng. 150 (4): 06024001. https://doi.org/10.1061/JWPED5.WWENG-2051.

Poppe, L. J. 2003. "ARMSTRONG74: Sediment Data from Great Bay Estuary, New Hampshire." Woods Hole, MA.: U. S. Geological Survey, Coastal and Marine Geology Program, Woods Hole Field Center.

Pröber, C. 1981. "Die Möglichkeit Der Fernerkundung in Der Küstengeologie. Eine Untersuchung Am Beispiel Der Nordfriesischen Wattsedimente Und Der Schwebfracht in Der Nordsee."

Swift, M. R, and W. S. Brown. 1983. "Distribution of Bottom Stress and Tidal Energy Dissipation in a Well-Mixed Estuary." Estuar. Coast. Shelf Sci., 17 (3): 297–317. https://doi.org/10.1016/0272-7714(83)90024-0.

Ulaby, F. T., R. K. Moore, and A. K. Fung. 1986. Microwave Remote Sensing: Active and Passive, Volume 3 Volume Scattering and Emission Theory, Advanced Systems and Applications. Reading, M.A.: Addison-Wesley.

van der Wal, D., P. M. J. Herman, and A. Wielemaker-Van Den Dool. 2005. "Characterisation of Surface Roughness and Sediment Texture of Intertidal Flats Using ERS SAR Imagery." Remote Sens. Environ., 98 (1): 96–109. https://doi.org/10.1016/j.rse.2005.06.004.

Veci, L. 2019. "SENTINEL-1 Toolbox SAR Basics Tutorial."

WillyWeather. 2023. "Piscataqua River - Mast Cove." WillyWeather. 2023. https://tides.willyweather.com/me/york-county/piscataqua-river--mast-cove.html.